

Ground-state properties of nanographite systems with zigzag-shaped edges

Toshiya Hikihara and Xiao Hu

Computational Materials Science Center, National Institute for Materials Science, Tsukuba, Ibaragi 305-0047, Japan

Hsiu-Hau Lin^{1,2} and Chung-Yu Mou¹

¹ *Department of Physics, National Tsing-Hua University, Hsinchu 300, Taiwan*

² *Physics Division, National Center for Theoretical Science, Hsinchu 300, Taiwan*

(Dated: October 30, 2018)

A π -electron network in nanographite systems with zigzag edges exhibits strongly localized edge states, which are expected to have peculiar properties. We study effects of electron-electron interactions on ground-state properties of the systems by means of the weak-coupling renormalization group and the density-matrix renormalization-group method. It is shown that the ground state is a spin-singlet Mott insulator with finite charge and spin gaps. We also find that the edge states are robust against the electronic correlations, resulting in edge effective spins which can flip almost freely. The schematic picture for the low-energy physics of the systems is discussed.

PACS numbers: 71.10.Hf, 73.22.-f, 75.75.+a

I. INTRODUCTION

Since the discoveries of fullerenes¹ and carbon nanotubes (CNTs),² the nature of “nanographites”, graphite-based materials with nano-meter sizes, has attracted much attention from both fundamental science and applications. One of the most striking features of the materials is a wide variety of properties they show depending on their geometrical structure, i.e., size, shape, surface condition and so on. For example, CNTs can be either metallic or semiconducting depending on the wrapping superlattice vector.³ Such a diversity of possible functions realized in nanographites makes them promising candidates for nano-scale devices.

Recently, it has been pointed out that a π -electron system in nanographites with zigzag-shaped edges exhibits peculiar electronic states strongly localized around the edges, which are termed “edge states”.^{4,5,6} Such a state does not appear around armchair-shaped edges. The nature of the edge states has been studied in the graphene sheet of nano-meter width, named the “nanographite ribbon” (NGR). Applying a tight-binding model for the NGR with zigzag edges, Fujita *et al.* have shown that the system has the electronic states localized on the edges, which penetrate from the edges into the bulk decaying exponentially.^{4,5} The edge states are believed to be responsible for a paramagnetic behavior observed in activated carbon fibers, which are taken to be an assembly of nanographite particles.^{7,8}

Since the edge states are characterized by almost flat dispersions in a certain range of the momentum space, which result in a sharp peak in the density of state at the Fermi energy, possible instabilities to various perturbations are important and have been investigated to date. Concerning the Peierls instability due to electron-phonon interactions, it has been shown that no bond alternation occurs in the zigzag NGRs with realistic interaction strength.⁹ On the other hand, effects of electron-electron interactions on the edge states have been investigated by

a mean-field approximation.^{4,10} The studies have shown that an infinitesimal on-site interaction causes a spontaneous spin polarization at the zigzag edges. Similar results have been obtained for the zigzag CNTs by the density-functional theory.^{11,12} However, it is also known that the one-body approximation adopted in these approaches is not appropriate for one-dimensional (1D) quantum systems such as NGRs and CNTs. In fact, Lieb’s theorem¹³ prohibits the spontaneous spin polarization for the Hubbard model in the nanographite systems with zigzag edges. More detailed analyses with controlled approximations are therefore desirable for clarifying the low-energy properties of the nanographites.

In this paper, we study effects of electron-electron interactions on the nanographite systems with zigzag edges using two powerful techniques: the weak-coupling renormalization group (RG) and the density-matrix renormalization group (DMRG) method.¹⁴ These approaches allow us to treat the strong quantum fluctuations in a controlled way for the 1D systems such as NGRs and CNTs. With the inclusion of electronic correlations, we show that the ground state of the zigzag NGR is a gapped spin-singlet and the artificially broken symmetry of spin rotations in the mean-field type analysis is restored by quantum fluctuations. It is rather interesting that the edge states survive in the presence of electron-electron interactions and play a crucial role in the low-energy regime.

The rest of this paper is organized as follows. The model is presented in the next section. In Sec. III, we show results of the weak-coupling analysis. We first discuss properties of the tight-binding model of the NGR system. Analytical eigen-wavefunctions and the corresponding energy spectrum are shown. And then, by keeping the low-lying edge states only and taking the electron-electron couplings into account, we derive the low-energy effective Hamiltonian in the continuum limit. It is shown that all coupling terms included in the Hamiltonian are relevant because of a large dynamical exponent

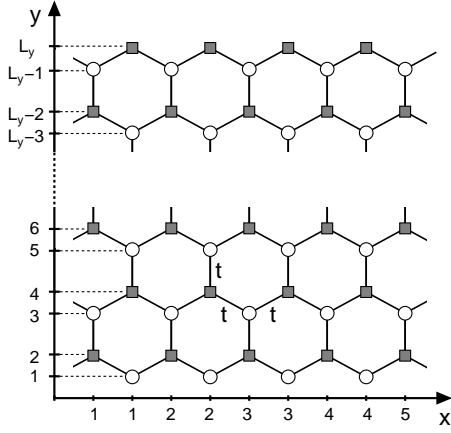


FIG. 1: Honeycomb lattice of carbon atoms in the zigzag NGRs and CNTs. The open circles and gray squares represent carbon sites of sublattice A and B, respectively.

of the dispersion of the edge states. The enhanced density of states at the Fermi energy generates finite charge and spin gaps, and consequently, the system exhibits a spin-singlet ground state without spontaneous symmetry breaking. The DMRG results are presented in Sec. IV. We find that in the presence of the Hubbard interaction the ground state is a spin singlet with finite charge and spin gaps, and no spontaneous spin polarization appears. Besides, electrons around the zigzag edges correlate ferromagnetically to compose effective spins which are easily polarized by applying an external field, while electrons in the bulk form a spin-singlet state which are hardly magnetized. The effective spins are localized around the zigzag edges even for a rather strong coupling, showing that the localization character of the edge states persists robustly against the electron-electron interactions. The schematic picture for the low-energy physics of the systems is discussed. Finally, our results are summarized in Sec. V.

II. MODEL HAMILTONIAN

In this paper, we consider a π -electron system at half-filling on a honeycomb lattice with zigzag edges as shown in Fig. 1. The effect of electron-electron couplings is incorporated by introducing the on-site Hubbard interaction U . The Hamiltonian is

$$\mathcal{H} = \mathcal{H}_0 + \mathcal{H}_U, \quad (1)$$

$$\mathcal{H}_0 = - \sum_{\mathbf{r}, \mathbf{r}'} \sum_{\alpha=\uparrow, \downarrow} t(\mathbf{r}, \mathbf{r}') [c_{\alpha}^{\dagger}(\mathbf{r}) c_{\alpha}(\mathbf{r}') + h.c.], \quad (2)$$

$$\mathcal{H}_U = U \sum_{\mathbf{r}} n_{\uparrow}(\mathbf{r}) n_{\downarrow}(\mathbf{r}), \quad (3)$$

where $c_{\alpha}(\mathbf{r})$ ($c_{\alpha}^{\dagger}(\mathbf{r})$) is the fermion annihilation (creation) operator at the site $\mathbf{r} = (x, y)$ and $n_{\alpha}(\mathbf{r}) \equiv c_{\alpha}^{\dagger}(\mathbf{r}) c_{\alpha}(\mathbf{r})$. The definition of the site index is shown in Fig. 1. The

system size in the x - and y -directions are denoted by L_x and L_y , respectively. Within tight-binding approximation, the hopping amplitude $t(\mathbf{r}, \mathbf{r}')$ is assumed to be t between nearest-neighbor sites and otherwise 0. In the x -direction, the open boundary condition with $L_x \rightarrow \infty$ is imposed for the zigzag NGR while the periodic boundary condition is imposed for the zigzag CNT. In the y -direction, the open boundary condition is imposed on the zigzag edges. We set L_y to be even so that the system always has the reflection symmetry in the y -direction. All carbon sites at the edges are assumed to be terminated by hydrogen atoms.

We note that the system is bipartite and the number of sites in each sublattice is equal, $N_A = N_B$. At the natural filling, with one π -electron per site on average, the system is particle-hole symmetric. Thus, one can apply Lieb's theorem¹³ to the system, which prohibits spontaneous spin polarizations in the ground state.

III. RENORMALIZATION GROUP

A. Band structure

To study the system in the weak-coupling limit $U \ll t$, it is natural to consider the case of $U = 0$ and analyze the band structure first. We thus begin with diagonalizing the hopping Hamiltonian \mathcal{H}_0 . Since the Hamiltonian is translational invariant along the x -direction, we can perform the partial Fourier transformation,¹⁵

$$c_{\alpha}(k_x; y) = \frac{1}{\sqrt{L_x}} \sum_x \exp[-ik_x(x + \delta)] c_{\alpha}(x, y) \quad (4)$$

where $\delta = 1/2$ for $y = 0, 1 \pmod{4}$ and $\delta = 0$ for $y = 2, 3 \pmod{4}$. By the transformation, the hopping Hamiltonian \mathcal{H}_0 is mapped into bond-alternating chains decoupled from each other,

$$\begin{aligned} \tilde{\mathcal{H}}_0 &= \sum_{k_x} \tilde{\mathcal{H}}_0(k_x), \\ \tilde{\mathcal{H}}_0(k_x) &= - \sum_{y=1}^{L_y-1} \sum_{\alpha} \tilde{t}(y) [c_{\alpha}^{\dagger}(k_x; y+1) c_{\alpha}(k_x; y) + h.c.], \end{aligned} \quad (5)$$

where $\tilde{t}(y) = t_1 \equiv 2t \cos(k_x/2)$ if y is odd while $\tilde{t}(y) = t_2 \equiv t$ if y is even. It is important to note that the effective hopping t_1 depends on the momentum k_x , and consequently, the motions in the x - and y -directions are entangled.

Each of the bond-alternating chains is composed of two sublattices A (odd y) and B (even y). The hopping between these two sublattices lead to the coupled Harper equations,

$$-t_1 \phi(y_A) - t_2 \phi(y_A + 2) = E \phi(y_A + 1), \quad (6)$$

$$-t_2 \phi(y_A - 1) - t_1 \phi(y_A + 1) = E \phi(y_A), \quad (7)$$

where $y_A = 1, 3, 5, \dots, L_y - 1$ are the lattice points of sublattice A. The open boundary condition in the y -direction requires $\phi(L_y + 1) = 0$ and $\phi(0) = 0$. From the coupled Harper equations, the wavefunctions of the eigenstates and the corresponding energy spectrum can be obtained in an analytical form. For the chains with $t_1 > t_2$ ($|k_x| < 2\pi/3$), the wavefunction is given by

$$\Psi(k_x; y_A) \equiv \begin{pmatrix} \phi_{p_y}(y_A) \\ \phi_{p_y}(y_A + 1) \end{pmatrix} = \begin{pmatrix} \pm \sin[p_y y_A + \varphi(p_y)] \\ \sin[p_y(y_A + 1)] \end{pmatrix}, \quad (8)$$

where the extra phase φ , chosen to be in the range $0 \leq \varphi(p_y) < \pi/2$, depends on the magnitude of momentum p_y ,

$$\varphi(p_y) = \tan^{-1} \left[\frac{t_1 - t_2}{t_1 + t_2} \tan p_y \right]. \quad (9)$$

Finiteness of L_y causes the quantization of p_y which satisfies the following constraint

$$(L_y + 1)p_y + \varphi(p_y) = m\pi, \quad (10)$$

where m is an integer. The energy spectrum for these states is given by

$$E(k_x, p_y) = \pm \sqrt{t_1^2 + t_2^2 + 2t_1 t_2 \cos(2p_y)}. \quad (11)$$

Here we emphasize that the momentum in the y -direction, k_y , is no longer a good quantum number due to the open boundaries. However, the magnitude of the momentum p_y remains a good one and would be quite helpful for identifying dominating interactions later. Since the wavefunction Eq. (8) is extended into the bulk sites, we call the states “extended states”.

For the chains with $t_1 < t_2$ ($|k_x| > 2\pi/3$), peculiar localized states show up. One finds that there are only $L_y - 2$ extended states in Eq. (8). The missing two states are linear combinations of localized states near the edges with complex momentum $k_y = \pm\pi/2 \pm i\gamma$. The wavefunctions for these edge states are

$$\Psi(k_x; y_A) = e^{i\pi y_A/2} \begin{pmatrix} \pm \sinh[\gamma(L_y + 1 - y_A)] \\ \sinh[\gamma(y_A + 1)] \end{pmatrix}. \quad (12)$$

The imaginary part of the momentum $\gamma \neq 0$ is the inverse of localization length of the edge states and satisfies the constraint

$$(L_y + 1)\gamma = \tanh^{-1} \left[-\frac{t_1 + t_2}{t_1 - t_2} \tanh \gamma \right]. \quad (13)$$

It is clear that the nonzero solution of γ only exists when $t_1 < t_2$. The energy spectrum for these edge states is given by

$$E(k_x, \gamma) = \pm \sqrt{t_1^2 + t_2^2 - 2t_1 t_2 \cosh(2\gamma)}. \quad (14)$$

We thereby obtain the whole band structure of the tight-binding Hamiltonian, Eqs. (11) and (14). The band

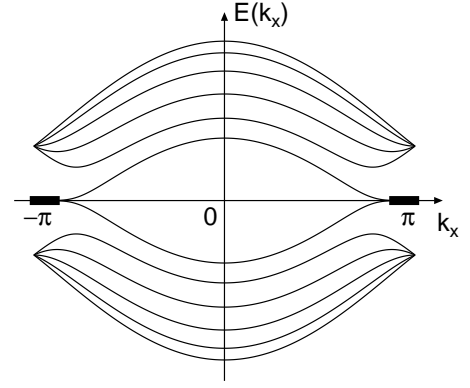


FIG. 2: Band structure of the zigzag NGR with $L_y = 12$. The bold lines represent dispersions around the Fermi point, $k_x = \pi$.

structure for $L_y = 12$ is shown in Fig. 2, as an example. It is worth noticing that the energy spectrum of the edge states is always lower than those of the extended states. It means that the edge states would dominate the low-energy physics in the weak-coupling limit while the extended states in the bulk do not play a crucial role because all of them are suppressed by a finite gap of order t/L_y .

B. Renormalization group analysis

Now, we are ready to treat the interacting Hamiltonian \mathcal{H}_U . After the partial Fourier transformation, the interacting Hamiltonian is written as,

$$\tilde{\mathcal{H}}_U = \frac{U}{L_x} \sum_{\{k_{x_i}\}} \sum_{y=1}^{L_y} \delta(k_{x_1} - k_{x_2} + k_{x_3} - k_{x_4}) \times c_{\uparrow}^{\dagger}(k_{x_1}; y) c_{\uparrow}(k_{x_2}; y) c_{\downarrow}^{\dagger}(k_{x_3}; y) c_{\downarrow}(k_{x_4}; y). \quad (15)$$

The delta function represents the momentum conservation in the x -direction. The Hamiltonian can be rewritten in terms of the eigenstates of $\tilde{\mathcal{H}}_0$ by expanding the electron operator on the diagonal basis,

$$c_{\alpha}(k_x; y) = \sum_p \phi_p(y) \psi_{p\alpha}(k_x). \quad (16)$$

where \sum_p is taken for all the extended states $p = p_y$ and, if ever, the edge states $p = \pm\gamma$. The resultant Hamiltonian is

$$\tilde{\mathcal{H}}_U = \frac{U}{L_x} \sum_{\{k_{x_i}\}} \sum_{\{p_i\}} \delta(k_{x_1} - k_{x_2} + k_{x_3} - k_{x_4}) \times \sum_y [\phi_{p_1}^*(y) \phi_{p_2}(y) \phi_{p_3}^*(y) \phi_{p_4}(y)] \times \psi_{p_1\uparrow}^{\dagger}(k_{x_1}) \psi_{p_2\uparrow}(k_{x_2}) \psi_{p_3\downarrow}^{\dagger}(k_{x_3}) \psi_{p_4\downarrow}(k_{x_4}). \quad (17)$$

In general, p_i are incommensurate and the dominant contribution comes from the pairwise equal p_i vertices while other kinds of vertices only occur in a limited tiny phase space. This great reduction of dominant interactions enables us to classify them into three categories. (i) The interactions involving only the edge states: Since the normalized wavefunction of the edge states is order one near the edge and vanishingly small in the bulk, the wavefunction product of $\phi_{p_i}(y)$ in Eq. (17) after summation over y is order one. Thus the edge-edge interaction remains $\mathcal{O}(U)$. (ii) The interactions involving a pair of the extended states and a pair of the edge states: Due to the spreading of wavefunction in the extended state, the summation of the wavefunction product in Eq. (17) is roughly $|\phi_{p_y}(1)|^2 \sim 1/L_y$. The edge-bulk interaction is therefore only $\mathcal{O}(U/L_y)$ and becomes smaller as the width of the NGR grows. (iii) The interactions involving only the extended states: From the similar argument to the case of the edge-bulk interaction, the bulk-bulk interaction turns out to be $\mathcal{O}(U)$. The effect of this interaction in the bulk system ($L_y \rightarrow \infty$) has been studied in Refs. 15 and 16 by the weak-coupling analysis. It has turned out that the interaction opens a finite energy gap even if the noninteracting Hamiltonian $\tilde{\mathcal{H}}_0$ includes gapless chains with $k_x = \pm 2\pi/3$.

Let us move on to deriving the low-energy effective Hamiltonian in the continuum limit. In the weak-coupling limit, the effective theory is dominated by the low-lying edge states near $k_x \approx \pi$ because all other bands in the bulk are gapped. Thus, we may keep only the edge states and neglect all the gapped modes. That is to say, only the kinetic energy of the edge modes and the edge-edge interaction term must be considered in the limit. It is useful to construct the antibonding and bonding fields $\psi_{\pm\alpha}(x)$ from the field for the edge states defined in Eq. (16),

$$\psi_{\pm\alpha}(x) = \int_{-\Lambda}^{\Lambda} \frac{dk_x}{2\pi} e^{ik_x x} \psi_{\pm\alpha}(k_x + \pi), \quad (18)$$

$$\psi_{\pm\alpha}(k_x) = \frac{1}{\sqrt{2}} [\psi_{+\gamma\alpha}(k_x) \pm \psi_{-\gamma\alpha}(k_x)], \quad (19)$$

where Λ is a momentum cutoff. Furthermore, we approximate the energy spectrum near $k_x \approx \pi$ to the lowest non-vanishing order $E_{\pm}(k) \simeq \pm c(k_x - \pi)^z$, where the \pm signs stand for the antibonding and bonding edge modes and the dynamical exponent $z = L_y - 1$. The kinetic energy can then be expressed in terms of the fields $\psi_{\pm\alpha}(x)$ in the continuum limit

$$\tilde{\mathcal{H}}_0 = \int dx \sum_{P=\pm} P \psi_{P\alpha}^\dagger(x) (-i\partial_x)^z \psi_{P\alpha}(x), \quad (20)$$

where the constant c is set to unity for notation simplicity.

While it is rather straightforward to write down the kinetic terms in the form of Eq. (20), expressing the edge-edge interaction in terms of the field operators is far from trivial. Our strategy to go from lattice to continuum limit

is to express the lattice operator for electrons in the edge states, $\tilde{c}_\alpha(x, y)$, in terms of the field operator $\psi_{\pm\alpha}(k)$ and relate it to $\psi_{\pm\alpha}(x)$ by Fourier transformation. To achieve the goal, we need to express $\tilde{c}_\alpha(x, y)$ in the eigenbasis of $\tilde{\mathcal{H}}_0$,

$$\tilde{c}_\alpha(x, y) = \int \frac{dk_x}{2\pi} e^{ik_x x} \sum_{P=\pm} \phi_P^*(y) \psi_{P\alpha}(k). \quad (21)$$

Here a difficulty comes from the entanglement of summation over k_x and P . Since γ depends on the longitudinal momentum k_x as in Eq. (13), the wavefunction $\phi_P(y)$ also has an implicit dependence on k_x . As a result, the lattice operator $\tilde{c}_\alpha(x, y)$ is not simply related to the continuous field $\psi_{\pm\alpha}(k)$ by Fourier transformation which requires the change of order between the summation over P and the integral over k_x . However, since the edge states with $k_x \simeq \pi$ are localized near the edges, it is reasonable to adapt the “sharp-edge” approximation which assumes that all the wavefunctions of the edge states take the simple form as for $k_x = \pi$, i.e.,

$$\phi_\pm(y) = \frac{1}{\sqrt{2}} (\delta_{y,1} \pm \delta_{y,L_y}). \quad (22)$$

Within the sharp-edge approximation, the relation between the lattice and the field operators becomes very simple,

$$\tilde{c}_\alpha(x, 1) = \frac{e^{i\pi x}}{\sqrt{2}} [\psi_{+\alpha}(x) + \psi_{-\alpha}(x)], \quad (23)$$

$$\tilde{c}_\alpha(x, L_y) = \frac{e^{i\pi x}}{\sqrt{2}} [\psi_{+\alpha}(x) - \psi_{-\alpha}(x)], \quad (24)$$

$$\tilde{c}_\alpha(x, y) = 0 \quad (2 \leq y \leq L_y - 1). \quad (25)$$

By substituting Eqs. (23) - (25) into the edge-edge interacting Hamiltonian

$$\mathcal{H}_{ee} = U \sum_r \tilde{c}_\uparrow^\dagger(x, y) \tilde{c}_\uparrow(x, y) \tilde{c}_\downarrow^\dagger(x, y) \tilde{c}_\downarrow(x, y), \quad (26)$$

we obtain its continuum counterpart,

$$\begin{aligned} \tilde{\mathcal{H}}_{ee} &= g_c(J_+^2 + J_-^2) + g_\rho J_+ J_- - g_\sigma \mathbf{J}_+ \cdot \mathbf{J}_- \\ &+ \frac{g_u}{2} (I_+ I_-^\dagger + I_- I_+^\dagger). \end{aligned} \quad (27)$$

Here the $SU(2)$ invariant currents are defined as

$$J_P \equiv \frac{1}{2} \psi_{P\alpha}^\dagger \psi_{P\alpha}, \quad (28)$$

$$\mathbf{J}_P \equiv \frac{1}{2} \psi_{P\alpha}^\dagger \boldsymbol{\sigma}_{\alpha\beta} \psi_{P\beta}, \quad (29)$$

$$I_P \equiv \frac{1}{2} \psi_{P\alpha}^\dagger \epsilon_{\alpha\beta} \psi_{P\beta}, \quad (30)$$

where $\boldsymbol{\sigma}$ and $\epsilon_{\alpha\beta}$ denotes Pauli matrices and an antisymmetric tensor, respectively. The bare values of these couplings generated by the on-site interaction U are $g_c = g_\rho = g_\sigma = g_u = U$. We note that Eq. (27)

is the most general form of the interacting Hamiltonian which includes four-fermion interactions with preserving the $U(1) \times SU(2)$ symmetry and the momentum conservation. In fact, one can use Eq. (27) to consider more complicated short-range interaction, which would generate a different set of bare couplings.

Finally, the low-energy field theory of the zigzag NGR in the continuum limit is described by Eqs. (20) and (27). At the tree level, the scaling dimensions of the all four-fermion interactions are $d(g) = z - 1$ by simple dimension counting. Since the dynamical exponent is greater than one for the NGR, all the couplings g_c, g_ρ, g_σ , and g_u are relevant under the RG transformation. However, we note that relevance of these couplings does not necessarily warrant excitation gaps in the energy spectrum. To identify the ground state, it is necessary to apply another approach such as the bosonization technique. We will discuss it in the next subsection.

C. Mott insulating ground state

In this subsection, we consider what we can derive from the low-energy effective Hamiltonian obtained in the previous subsection. One clue is the fact that the effective Hamiltonian has a form strikingly similar to the usual effective theory for 1D systems except for the large dynamical exponent $z > 1$. Hence, we discuss the analogy between the NGRs and a one-chain system to derive the ground-state properties of the NGR. On the other hand, the spectrum of the low-lying edge states in the NGR can be viewed as a two-chain system, whose bonding and antibonding bands touch the Fermi energy at one Fermi point as discussed below. Therefore, it is also useful to consider the NGR in the analogy with the two-chain system. We will see that the both analyses give the same conclusion: the NGR has a spin-singlet ground state with finite charge and spin gaps.

Let us start with the first approach, i.e., considering the NGR in the analogy to a one-chain system at half-filling. In this analogy, the field $\psi_{+\alpha}$ ($\psi_{-\alpha}$) is regarded as a right- (left-) moving field operator. Since the dispersion of the fields $\psi_{\pm\alpha}(x)$ is not linear, the rigorous mapping from the fermionic theory to the bosonic one is not possible. However, it is likely that the large dynamical exponent z just serves to make all interactions relevant and we can still use the bosonization techniques to clarify physical properties of the ground states qualitatively. That is to say, we can treat the dynamical exponent $z = 1 + \epsilon$ as a perturbation and still use the conventional bosonization rules to study the physical properties of the NGRs. Under the assumption, we follow conventional bosonization steps and introduce two pairs of bosonic fields

$$\psi_{\pm\alpha}(x) \simeq \sqrt{\rho} e^{i[\phi_\alpha(x) \pm \theta_\alpha(x)]/2}, \quad (31)$$

where $\phi_\alpha(x)$ and $\theta_\alpha(x)$ are respectively the phase and displacement fluctuations, which obey the commutation

phase	$(\sqrt{2}\theta_\sigma, \sqrt{2}\theta_\rho)$	C_s	D
New	$(\pi, 0)$	0	0
CDW	$(0, \pi)$	$\neq 0$	0
Dimer	$(0, 0)$	0	$\neq 0$

TABLE I: Comparison between different phases.

relation,

$$[\phi_\alpha(x), \theta_{\alpha'}(x')] = -2\pi i [1 + \text{sign}(x - x')] \delta_{\alpha\alpha'}. \quad (32)$$

Furthermore, we switch to the charge and spin basis defined by

$$(\phi_{\rho,\sigma}, \theta_{\rho,\sigma}) = \frac{1}{\sqrt{2}} [(\phi_\uparrow, \theta_\uparrow) \pm (\phi_\downarrow, \theta_\downarrow)]. \quad (33)$$

The effective interaction which is relevant to gap formation in Eq. (27) can be written down in terms of these bosonic fields,

$$\tilde{H}_{ee} = g_\sigma \cos(\sqrt{2}\theta_\sigma) - g_u \cos(\sqrt{2}\theta_\rho). \quad (34)$$

The absence of their dual fields ϕ_ρ and ϕ_σ in the interactions comes from the charge and spin conservations. For the on-site interaction, both g_σ and g_u are positive and grow under RG transformation. Consequently, the corresponding bosonic fields are pinned at specific values up to fluctuations,

$$\sqrt{2}\theta_\sigma \simeq \pi, \quad \sqrt{2}\theta_\rho \simeq 0. \quad (35)$$

The signs of the couplings are of crucial importance here. Expanding the cosine term around the pinned values, the system acquires finite gaps in both charge and spin sectors. Therefore, the ground state is a Mott insulator with both charge and spin gaps. The formation of the charge gap is not surprising because the electron density is commensurate with the underlying lattice structure. The finite spin gap indicates that the spin rotational symmetry is not broken spontaneously and the ground state is a spin singlet, as predicted by Lieb's theorem. The result differs from the mean-field theory predictions where the quantum fluctuations are ignored. We believe that the strong fluctuations in 1D systems would invalidate the mean-field approach and restore the symmetry which is broken at the mean-field level.

It is worth noting that for the usual weakly-coupled 1D system with linear energy spectrum, the bosonic fields never get pinned at the values listed in Eq. (35) because it is not stable in the RG flow. However, the new phase here is stable due to the large dynamical exponent which corresponds to the van Hove singularity in the density of states. We summarize the pinned values for each phase in Table I. To differentiate this new phase from the familiar charge density wave or the dimer phase, one needs to compute the order parameters, i.e., charge density modulation C_s and bond dimerization D defined as

$$C_s \equiv (-1)^x \langle a_\alpha^\dagger(x) a_\alpha(x) \rangle$$

$$\simeq \langle \psi_{+\alpha}^\dagger \psi_{-\alpha} \rangle + \langle \psi_{-\alpha}^\dagger \psi_{+\alpha} \rangle, \quad (36)$$

$$D \equiv \frac{(-1)^x}{2} \langle a_\alpha^\dagger(x) a_\alpha(x+1) + a_\alpha^\dagger(x+1) a_\alpha(x) \rangle$$

$$\simeq -i \langle \psi_{+\alpha}^\dagger \psi_{-\alpha} \rangle + i \langle \psi_{-\alpha}^\dagger \psi_{+\alpha} \rangle, \quad (37)$$

where $a_\alpha(x)$ is the lattice operator in the one-chain system and related to the fields as $a_\alpha(x) \simeq e^{ik_F x} \psi_{+\alpha}(x) + e^{-ik_F x} \psi_{-\alpha}(x)$ with $k_F = \pi/2$. Using the relations

$$\psi_{+\uparrow}^\dagger \psi_{-\uparrow} \simeq i e^{-i\theta_\rho/\sqrt{2}} e^{-i\theta_\sigma/\sqrt{2}}, \quad (38)$$

$$\psi_{+\downarrow}^\dagger \psi_{-\downarrow} \simeq i e^{-i\theta_\rho/\sqrt{2}} e^{+i\theta_\sigma/\sqrt{2}}, \quad (39)$$

and substituting the pinned values of the bosonic fields, one obtain the expectation values of the order parameters. The results are listed in Table I. It is clear that there is no long-range order or symmetry breaking for the ground state of the zigzag NGRs.

Now we take another perspective and view the NGR as a system of two chains coupled via an interchain hopping. Figure 3 (a) shows the band structure of the two-chain system for the special point $t_{\text{runc}}/t_{\text{leg}} = 2$, where t_{runc} (t_{leg}) is an amplitude of the interchain (intrachain) hopping. As the hoppings are tuned at the special value, the chemical potential cut through the bonding (antibonding) band at single Fermi point $k_x = \pi$ ($k_x = 0$) with vanishing Fermi velocity $v_F \rightarrow 0$, rather than two pairs of Fermi points in general. On the other hand, both the bonding and antibonding bands of the low-lying edge states in the NGRs have single Fermi point $k_x = \pi$ with $v_F \rightarrow 0$. Hence, in the low-energy limit, the peculiar band structure in the NGRs can be viewed as a two-chain system with shifting the momentum of the antibonding field $k_x \rightarrow k_x + \pi$ [See Fig. 2 and Fig. 3 (b)]. One might worry that the dynamical exponent in the NGRs $z = L_y - 1$ may be different from that in the two-chain system $z = 2$. However, the dynamical exponent z in this limit only affects how the Fermi velocity approaches zero and should not give rise to qualitative difference.

In the weak-coupling limit, the lattice electron operator $a_{i\alpha}(x)$ in the i -th chain of the two-chain system can be described by two pairs of chiral fields

$$a_{1\alpha}(x) = \frac{e^{i\pi x}}{\sqrt{2}} [\psi_{+\alpha}(x) + e^{iQx} \psi_{-\alpha}(x)], \quad (40)$$

$$a_{2\alpha}(x) = \frac{e^{i\pi x}}{\sqrt{2}} [\psi_{+\alpha}(x) - e^{iQx} \psi_{-\alpha}(x)], \quad (41)$$

where $Q = \pi$ is the momentum difference between Fermi points of bonding and antibonding bands in the two-chain system. The relation of lattice operators to the field operators for the two-chain system in Eqs. (40) and (41) are strikingly similar to those for the NGR in Eqs. (23) and (24), except the momentum shift Q . This enables us to translate the excitations and correlations in the two-chain system directly into those for the NGRs.

For on-site repulsive interaction, the ground state of the two-chain system is the Mott insulator with finite

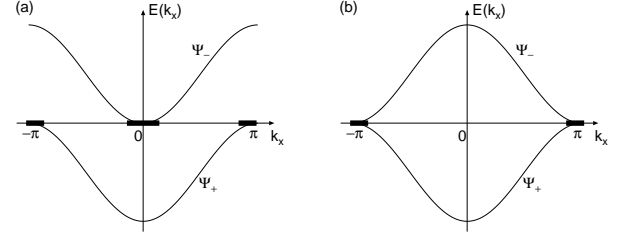


FIG. 3: Schematic picture of the band structure of (a) the two-chain system with $t_{\text{runc}}/t_{\text{leg}} \rightarrow 2$, and (b) the same system with the momentum shift $Q = \pi$ for the antibonding field. The bold lines represent dispersions around Fermi points.

charge and spin gaps. In addition, there exists neither broken symmetry nor local order parameter. This Mott-insulating phase resembles the peculiar phase we discussed above by making analogy to the one-chain case. Thus, both approaches support that the ground state of the NGRs is a spin singlet with finite charge and spin gaps.

The two-chain analogy also gives us information about the spin-spin correlation. It is known that the two-chain system has magnon excitations with spin $S = 1$ and momentum $P = (\pi, \pi)$. The momentum shift Q in the x -direction shifts the low-lying magnon to $P = (0, \pi)$. This means that the spin-spin correlation functions in the NGRs are ferromagnetic within the same edge and antiferromagnetic between opposite edges. This result is consistent with the fact that the sites in the same edge belong to the same sublattice while those in opposite edges belong to different sublattices.

IV. NUMERICAL RESULTS

In this section, we present numerical results for the π -electron system (1) at half-filling. Hereafter, we set $t = 1$. Using the DMRG method with improved algorithm,^{14,17} we have calculated various energy gaps and correlation functions. The number of kept states is up to $m = 1200$ per block. Numerical errors due to the truncation of the DMRG calculation are estimated from the difference between the data with different m 's. We discuss the results for the zigzag NGRs and the zigzag CNTs in the following subsections.

A. Zigzag nanographite ribbons

In this subsection, we show results on the zigzag NGRs. We first discuss the results for $L_y = 4$. In all the cases calculated, we have found that the ground state belongs to the subspace of $M = 0$, where M is the total magnetization in the system. In Fig. 4, we show the data of the

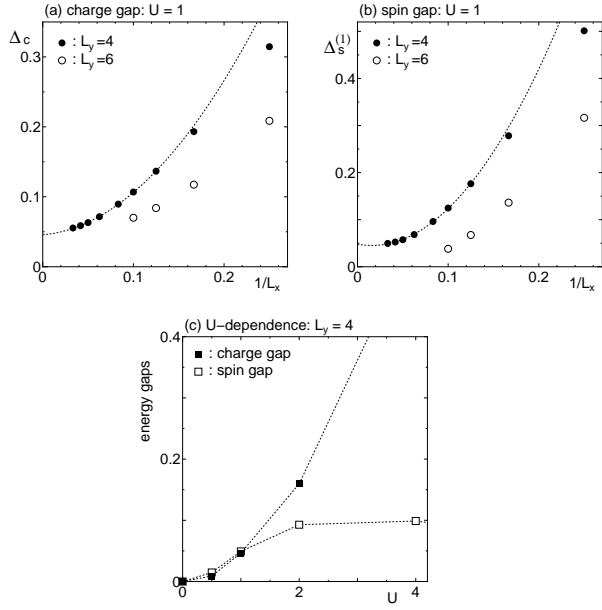


FIG. 4: L_x -dependence of the energy gaps in the NGRs for $U = 1$; (a) the charge gap Δ_c , (b) the spin gap $\Delta_s^{(1)}$. The solid and open circles represent the data for $L_y = 4$ and $L_y = 6$, respectively. The numerical errors due to the DMRG truncation are smaller than symbols. The gaps for $L_y = 4$ are extrapolated by fitting the data to a polynomial form, $\Delta(L_x) = \Delta(\infty) + a/L_x + b/L_x^2$ where a and b are fitting parameters. (c) The U -dependence of the extrapolated gaps for $L_y = 4$.

charge and spin gaps defined as

$$\Delta_c = \frac{1}{2} \left[E_0 \left(\frac{N}{2} + 1, \frac{N}{2} \right) + E_0 \left(\frac{N}{2} - 1, \frac{N}{2} \right) - 2E_0 \left(\frac{N}{2}, \frac{N}{2} \right) \right], \quad (42)$$

$$\Delta_s^{(M)} = E_0 \left(\frac{N}{2} + M, \frac{N}{2} - M \right) - E_0 \left(\frac{N}{2}, \frac{N}{2} \right) \quad (43)$$

where $E_0(N_\uparrow, N_\downarrow)$ is the lowest energy in the subspace of N_\uparrow up-spin and N_\downarrow down-spin electrons and N is the total number of sites. For $L_y = 4$, both the energy gaps are extrapolated to non-zero values at $L_x \rightarrow \infty$. The U -dependence of the extrapolated gaps suggests that both of the gaps start to open from infinitesimal U , i.e., $U_c = 0$. We thus conclude that for arbitrary $U > 0$ the ground state of the zigzag NGRs is a spin singlet with finite charge and spin gaps, being consistent with the weak-coupling analysis.

To see how the spin polarizations are distributed in real space, we have calculated the local spin polarization

$$\langle S^z(\mathbf{r}) \rangle_M = \frac{1}{2} \langle n_\uparrow(\mathbf{r}) - n_\downarrow(\mathbf{r}) \rangle_M, \quad (44)$$

where $\langle \cdots \rangle_M$ denotes the expectation value in the lowest-energy state in the subspace of M . We have found that in

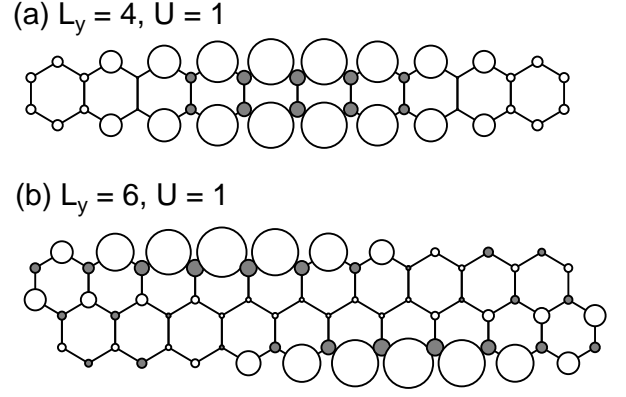


FIG. 5: Distribution of local spin polarization $\langle S^z(\mathbf{r}) \rangle_{M=1}$ in the NGRs with (a) $L_y = 4$ and (b) $L_y = 6$. The Hubbard coupling and the total magnetization are $U = 1$ and $M = 1$. Open and gray circles respectively represent the positive and negative values of the spin polarization while the areas of them are proportional to the magnitude.

the ground state the local spin polarization $\langle S^z(\mathbf{r}) \rangle_{M=0}$ is zero at all sites within the numerical error, supporting that the ground state is spin singlet. There is no spontaneous spin polarization. Figure 5 (a) shows the distribution of the local spin polarization in the magnetized state of $M = 1$ for $U = 1$ and $L_y = 4$. As seen in the figure, the magnetization appears almost only at the edge sites. This suggests that the electrons in the edge states are polarized by an external field more easily than those in the bulk. We note that the localization character of the magnetization seems to persist even for a rather large coupling $U = 4$. In other words, the edge states survive robustly against the electron-electron interactions even if U becomes larger than the hopping amplitude t .

In Fig.6, we show the spin-spin correlation functions in the edge sites,

$$\langle S^z(x, 1) S^z(x', 1) \rangle_{M=0}. \quad (45)$$

To reduce boundary effects, the correlations are calculated between the sites of the same distance from the center of the NGR. The correlations turn out to be always positive, suggesting a ferromagnetic coupling between the sites in the same edge. We have also found that the spin correlation between the sites in opposite edges is always negative, i.e., antiferromagnetic. These behaviors are consistent with the expectation from the two-chain analogy discussed above. The correlations decay exponentially for all U 's reflecting the finite spin gap,¹⁹ and are enhanced as U increases.

Finally, we discuss the dependence of low-energy properties of the zigzag NGRs on the width L_y . Since the low-energy physics of the NGRs is dominated by the edge states which are strongly localized around the zigzag edges, it is likely that the singlet-triplet spin gap $\Delta_s^{(1)}$, which corresponds to the energy scale required to magnetize the edge spins, comes from the antiferromagnetic

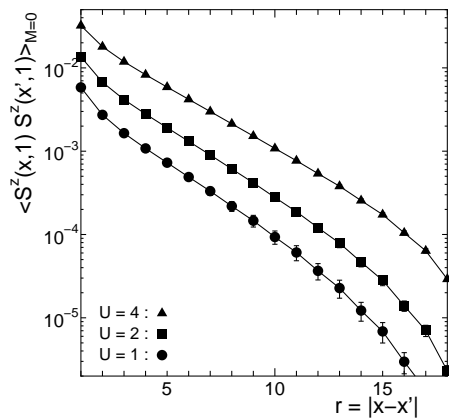


FIG. 6: Ground-state spin-spin correlation functions in the NGRs with $L_y = 4$ and $L_x = 20$. The circle, square, and triangle represent the data for $U = 1, 2$, and 4 , respectively. The error bars represent the numerical error due to the DMRG truncation.

effective coupling between the electrons in the edge states of opposite sides. Thus, it is natural to expect that the spin gap decreases as the width L_y increases. To see this, we have performed calculations for the NGR with $L_y = 6$.²⁰ As can be seen in Fig. 5 (b), the spin polarizations in the magnetized state of $M = 1$ are found to be strongly localized at the zigzag edges, suggesting that the edge states exist also for $L_y = 6$. Furthermore, we can clearly see in Fig. 4 that the spin gap for the same L_x decreases as the width of the ribbon L_y increases, as expected. Unfortunately, the system size calculated for $L_y = 6$ is not large enough to obtain the extrapolated gap $\Delta_s^{(1)}(L_x \rightarrow \infty)$. Calculations for larger systems are desirable to clarify the situation for the NGRs with larger L_y .

B. Zigzag nanotubes with open edges

For the zigzag CNTs with open ends, we can apply basically the same argument as that for the zigzag NGRs. The difference between the two systems is merely the fact that in the CNTs the momentum along the x -direction is quantized as $k_x = 2\pi n/L_x$ due to the finite circumference L_x . To see what happens, we have done calculations for the zigzag CNT with $L_x = 2$. In this case, there is one edge state at each zigzag open end. Although the width of the CNT is quite narrow, we will show that characteristic magnetic properties expected for general zigzag CNTs already appear.

We have found that the ground state always belongs to the subspace of $M = 0$ for all values of $U > 0$. In Fig. 7, we show the data of the charge gap Δ_c and the spin gaps $\Delta_s^{(1)}$ and $\Delta_s^{(2)}$. It can be seen in the figure that all the gaps take nonzero values in all the case of $U > 0$ and L_y calculated. We therefore conclude that the ground state of the zigzag CNTs with finite L_y is a spin-singlet Mott

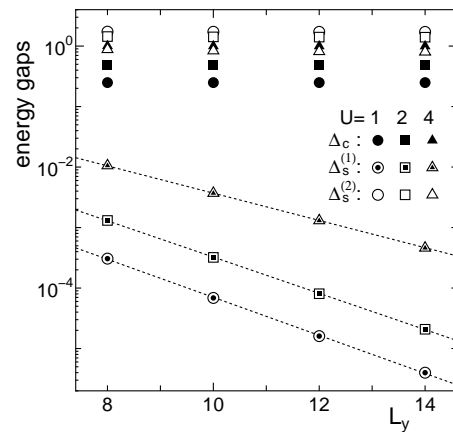


FIG. 7: Charge gap Δ_c and spin gaps $\Delta_s^{(1)}$ and $\Delta_s^{(2)}$ of the CNTs with $L_x = 2$ for $U = 1, 2$, and 4 as functions of the length of CNTs L_y . The numerical errors due to the DMRG truncation are smaller than symbols. The dotted lines are guides for eye.

insulator, same as the NGRs. An interesting observation here is that the spin gap $\Delta_s^{(1)}$ decays exponentially as L_y increases while $\Delta_s^{(2)}$ converges to finite values at $L_y \rightarrow \infty$. Hence, for large enough L_y , the magnetization $M = 1$ can be induced by applying an infinitesimal field whereas a finite field is needed to magnetize the system to $M \geq 2$.

Next, we discuss how the spin polarizations are distributed in real space. Same as the NGRs, the local spin polarization in the ground state is zero at all sites. Figure 8 shows the distribution of the local spin polarization $\langle S^z(\mathbf{r}) \rangle_M$ in magnetized states for $U = 1$. The data clearly show that in the state of $M = 1$ the induced magnetization are strongly localized at the ends of the zigzag CNT. This demonstrates the robustness of the localization character of the edge states against the coupling U . In the state of $M = 2$, on the other hand, the distribution of $\langle S^z(\mathbf{r}) \rangle_{M=2}$ seems to be a superposition of the edge magnetization and magnetization excited in the bulk sites. We have found similar distributions of $\langle S^z(\mathbf{r}) \rangle_M$ for $U = 2$ and 4 .

The results on the spin gaps and the local spin polarizations lead us to the conclusion that there are two different energy scales in magnetic excitations in zigzag CNTs: the energy to magnetize electrons in the edge states and the one to magnetize the bulk electrons. As the length of the CNT increases, the former decays exponentially while the latter converges to a finite value, the spin gap of the bulk system. This suggests that one can regard the edge states and the bulk electrons as two almost independent objects; The edge states are essentially decoupled from the bulk singlet state in spite of the presence of $U \simeq \mathcal{O}(t)$. Very recently, it has been pointed out from a weak-coupling analysis that thicker CNTs including more than one edge states at each open ends also exhibit such a decoupling of the edge and bulk states.²¹ We therefore expect that the conclusion above is valid

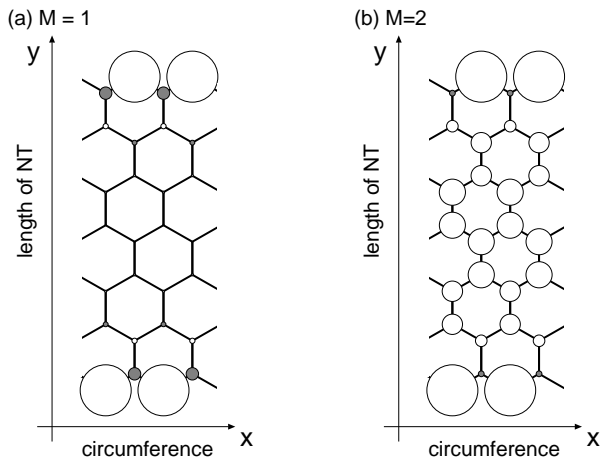


FIG. 8: Distribution of local spin polarization in the CNTs with $L_x = 2$ for $U = 1$ and $L_y = 14$. The total magnetization is (a) $M = 1$ and (b) $M = 2$. Open and gray circles respectively represent the positive and negative values of the spin polarization while the areas of them are proportional to the magnitude.

for general CNTs with zigzag open edges.

C. Picture of the low-energy states

From the above results, we can deduce a schematic picture to represent the low-energy physics of the zigzag NGRs and CNTs. In this picture, the π -electron system consists of two parts: the electrons in the bulk forming a spin-singlet state and those in the edge states at each zigzag edge. The electrons in the same edge are correlated ferromagnetically with each other to compose a large effective spin. The effective spins interact via an effective antiferromagnetic coupling across the bulk singlet state. Hence, the ground state of the system is a spin singlet in total. The effective coupling becomes smaller as the distance between the effective spins becomes larger, and finally, when the distance becomes large enough, the effective spins can flip freely, giving a paramagnetic response. The bulk electrons remain forming a spin singlet unless a field corresponding to the bulk spin gap is applied. We note that the picture above is basically consistent with the one discussed in Refs. 10 and 22.

V. DISCUSSION

In this paper, we have studied low-energy properties of nanographite systems with zigzag edges in the presence of

on-site Hubbard interactions U using the weak-coupling RG and the DMRG method. We have analyzed the Hubbard model on the zigzag NGRs and the zigzag CNTs. We find that in both systems the ground state for $U > 0$ is a spin-singlet Mott insulator with finite charge and spin gaps. It is also found that the localization property of the edge state persists even for a rather large value of U , resulting in the effective spins localized around the zigzag edges.

Finally we wish to touch upon further extensions of this study. One issue to be studied is effects of further hoppings and long-range electron-electron interactions. As for magnetism, these long-range terms violate the assumptions of Lieb's theorem and open the possibility of exotic magnetic states. However, it is also expected that the spin gap observed in the present study tends to stabilize the spin-singlet ground state against perturbations. Very recently, it has been pointed out by the density-functional theory¹² that zigzag CNTs with a finite length can exhibit a high-spin ground state depending on the circumference L_x , although the method may underestimate effects of strong quantum fluctuation in the nanographite systems. To clarify the situation, analyses with controlled approximations are needed. Another issue is stacking effects. Nanographite materials often take a stacking form, *e.g.*, nanographite particles composed by a few graphene sheets and multiwall CNTs. Hence, it is important for applications to study effects of interlayer interactions. For nanographite particles, it has been shown that their magnetic properties change drastically depending on types of stacking geometry.²³ In multiwall CNTs, the difference of radius and chirality between inner and outer layer is expected to affect not only the edge states but also the bulk properties in a complicated way. Further extensive studies are desirable to tackle the issue.

Acknowledgments

We are grateful to K. Wakabayashi and A. Tanaka for fruitful discussions. TH thanks S. Okada for sending a preprint before publication. TH and XH are supported by the Ministry of Education, Culture, Sports, Science and Technology, Japan, under the Priority Grant No. 14038240. HHL and CYM appreciate the financial support from National Science Council in Taiwan through grant Nos. 91-2112-M007-040 (HHL), 91-2120-M-007-001 (HHL) and 91-2112-M007-049 (CYM).

¹ H. Kroto *et al.*, Nature **318**, 162 (1985).

² S. Iijima, Nature **354**, 56 (1991).

³ For a review, see R. Saito, G. Dresselhaus and M.S. Dresselhaus, *Physical Properties of Carbon Nanotubes* (Impe-

- rial College Press, 1998).
- ⁴ M. Fujita, K. Wakabayashi, K. Nakada and K. Kusakabe, J. Phys. Soc. Jpn. **65**, 1920 (1996).
 - ⁵ K. Nakada, M. Fujita, G. Dresselhaus and M.S. Dresselhaus, Phys. Rev. B **54**, 17954 (1996).
 - ⁶ K. Wakabayashi, M. Fujita, H. Ajiki and M. Sigrist, Phys. Rev. B **59**, 8271 (1999).
 - ⁷ Y. Shibayama, H. Sato, T. Enoki and M. Endo, Phys. Rev. Lett. **84**, 1744 (2000).
 - ⁸ Y. Shibayama, H. Sato, T. Enoki, X-X. Bi, M.S. Dresselhaus and M. Endo, J. Phys. soc. Jpn. **69**, 754 (2000).
 - ⁹ M. Fujita, M. Igami and K. Nakada, J. Phys. Soc. Jpn. **66**, 1864 (1997).
 - ¹⁰ K. Wakabayashi, M. Sigrist and M. Fujita, J. Phys. Soc. Jpn. **67**, 2089 (1998).
 - ¹¹ S. Okada and A. Oshiyama, Phys. Rev. Lett. **87**, 146803 (2001).
 - ¹² S. Okada and A. Oshiyama, unpublished.
 - ¹³ E.H. Lieb, Phys. Rev. Lett., **62**, 1201 (1989).
 - ¹⁴ S.R. White, Phys. Rev. Lett. **69**, 2863 (1992); Phys. Rev. B **48**, 10345 (1993).
 - ¹⁵ H.-H. Lin, Phys. Rev. B **58**, 4963 (1998).
 - ¹⁶ L. Balents and M.P.A. Fisher, Phys. Rev. B **55**, R11973 (1997).
 - ¹⁷ S. R. White, Phys. Rev. Lett. **77**, 3633 (1996).
 - ¹⁸ T. Kennedy, J. Phys. Condens. Matter **2**, 5737 (1990).
 - ¹⁹ We note that the suppression of the correlation functions from the linear behavior seen for large $r \sim L_x$ is due to the presence of the open boundaries and is not essential.
 - ²⁰ For the NGR with $L_y = 6$, we remove the boundary sites $(x, y) = (1, L_y)$ and $(L_x, 1)$, which are connected to other site by only one bond, to avoid undesirable boundary effects. The shape of the system calculated is shown in Fig. 5 (b).
 - ²¹ S. Ryu and Y. Hatsugai, cond-mat/0211008.
 - ²² K. Nakada, M. Igami and M. Fujita, J. Phys. Soc. Jpn. **67**, 2388 (1998).
 - ²³ K. Harigaya, Chem. Phys. Lett. **340**, 123 (2001).